Journal of Inorganic and Organometallic Polymers and Materials (2023) 33:2058–2074
https://doi.org/10.1007/s10904-023-02653-5

RESEARCH

Effect of Solvent Assisted Linker Exchange (SALE) and De Novo Synthetic Routes on CO_2 Uptake and Fixation by Mixed-Linker Zeolitic Imidazolate Frameworks

Yuel W. Abraha[1] · Francois J. F. Jacobs[1] · Alice Brink[1] · Ernst H. G. Langner[1]

Received: 21 February 2023 / Accepted: 10 April 2023 / Published online: 20 April 2023

Abstract
Direct mixing (de novo) and Solvent Assisted Ligand Exchange (SALE) are the main methods used for the synthesis of Mixed-Linker Zeolitic Imidazolate Frameworks (ML-ZIFs). ML-ZIFs with combined $–NO_2$ and –Br/–Cl functionalities were prepared via both synthetic routes. Thereafter the CO_2 uptake of the ML-ZIFs were compared, as well as their abilities to fixate CO_2 with epoxide substrates. The de novo synthesis resulted in ML-ZIFs with SOD topologies, 60: 40 ($–NO_2$: –Br/–Cl) functionality ratios, higher porosities, better thermal stability and higher CO_2 uptake than equivalent SALE products. SALE resulted in smaller ML-ZIF crystallites, only ~ 10% incorporation of –Br/–Cl functionalized imidazolate linkers, and phase change during activation. ML-ZIF-7_{Cl}, obtained from direct mixing, resulted in the highest CO_2 uptake (90 $cm^3\ g^{-1}$), in line with its higher porosity. ML-ZIF-7_{Cl}, in combination with tetrabutylammonium bromide (TBAB), showed a high catalytic activity (TOF of 446 h^{-1}) for the fixation of CO_2 with propylene oxide and was reusable for up to 4 cycles without loss in activity.

✉ Ernst H. G. Langner
langneeh@ufs.ac.za

[1] Department of Chemistry, University of the Free State, Nelson Mandela Drive, P.O. Box 339, Bloemfontein 9300, South Africa

Graphical Abstract

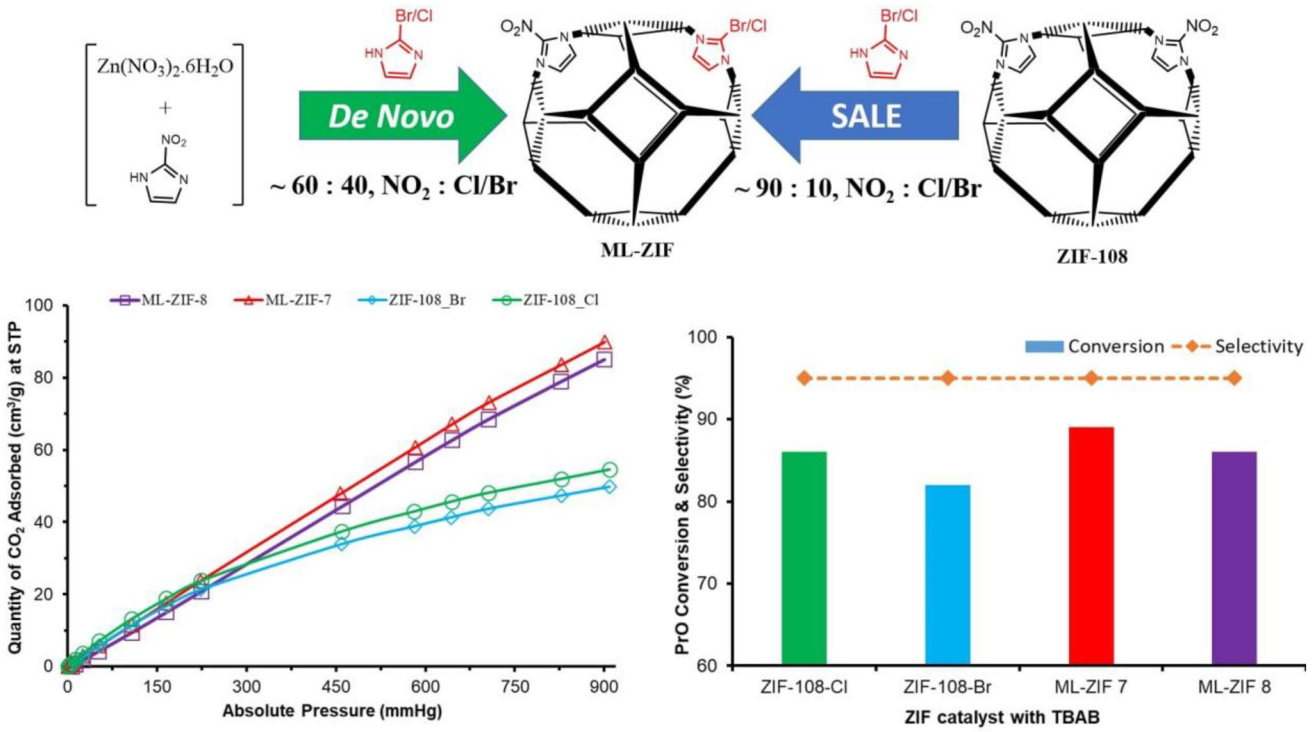

Keywords Zeolitic imidazolate frameworks (ZIFs) · Solvent assisted ligand exchange (SALE) · De Novo synthesis · CO_2 uptake · CO_2 fixation

1 Introduction

The removal of carbon dioxide from the atmosphere is essential in minimizing the impact of global warming due to the use of fossil fuels [1, 2]. In the last two decades, ZIFs, a subfamily of Metal–Organic Frameworks (MOFs), with divalent metal centres tetrahedrally connected by imidazolate-based linkers, have garnered much interest for CO_2 separation, adsorption/capture and utilization applications [3–5].

ZIFs have high porosity, tuneable functionality, high thermal and mechanical properties, making them ideal for industrial CO_2 capture and sequestration (CCS) as well as CO_2 capture and utilization (CCU) applications [6]. CCU technologies have the added advantage of valorizing CO_2 and compensating for CCS costs [7, 8]. The use of ZIF catalysts for forming cyclic carbonates through the cycloaddition of CO_2 with epoxide substrates is one type of CCU that has gained much attention recently for its green chemistry, 100% atom economy and high value-added products [9, 10]. Cyclic carbonates are valuable chemicals with applications in metal extraction, electrolytes in lithium-ion batteries and supercritical fluid separation [11, 12].

Extensive experimental and computational studies have shown that both CO_2 fixation and uptake by ZIFs are subject to the functionality of their linkers [13–16]. ZIFs with electron-withdrawing groups (EWG) achieved the highest CO_2 uptakes in the following order of linker functionality: $NO_2 > Cl > Br > CN > H > CH_3$ [17–19]. This has been attributed to the high quadrupole moment of ZIFs with EWG, resulting in a higher interaction of CO_2 and polar functionality [20]. The cycloaddition of CO_2 with epoxide substrates requires a catalyst with both Lewis acid (LA) and Lewis base (LB) sites, LAs open the epoxide ring, whereas LBs activate CO_2 [21, 22]. ZIFs are bifunctional catalysts with dual LA (–NH of imidazole linker) and LB (metal centre) sites, making them suitable for cycloaddition reactions [23].

The use of mixed–linker ZIFs with combined EWG ($–NO_2$) and electron-donating ($–CH_3$) functionalities has shown that Electron density (ED) symmetry also plays a part in the CO_2 uptake and fixation of ZIFs. Solvent Assisted Ligand Exchange (SALE) of ZIF-8 (with $Zn(CH_3Im)_2$ composition) with NO_2Im resulted in an asymmetric ED, which led to a 155% increase in CO_2 capacity of ZIF-8 [24, 25]. Similarly, ML-ZIF 3 with $Zn(mIm)_{0.82}(NO_2Im)_{1.18}$ composition has shown a 72% increase in CO_2 uptake compared

to. ZIF-108 (with only NO_2Im linkers) and a 140% increase compared to ZIF-8 (with only mIm linkers) [26, 27]. This study aims to combine the high-performing linker functionalities (–NO_2 and –Br/–Cl) on one ZIF structure and investigate its effect on CO_2 uptake and conversion.

There are two routes for a multi-linker ZIF synthesis: direct incorporation of the two linkers during the synthesis process (de novo) and post-synthetic modification (PSM) of a single-linker ZIF. The de novo method is a one-pot synthesis reaction, where the mixture of linkers is combined with the metal source. The crystal structure is then determined by how the two linkers compete in structure-directing and interact with each other [6]. SALE is a type of PSM, where a single-linker ZIF is reacted with an excess secondary linker in a suitable solvent system [28]. SALE occurs via a heterogeneous nucleation process, where the parent material is used as seeds [29]. To the best of our knowledge, this is the first report of de novo or SALE synthesis of ZIFs with combined 2-nitroimidazole (NO_2Im) and 2-bromoimidazole (BrIm)/2-chloroimidazole (ClIm) linkers, respectively.

Herein, we present a comparative study (thermal stability, linker ratio, topology, porosity, and CO_2 uptake) of de novo and SALE routes for synthesizing mixed-linker ZIFs with combined –NO_2 and –Br/Cl functionalities. In addition, the catalytic activities of de novo and SALE prepared ML-ZIFs in the fixation of CO_2 with an epoxide substrate are reported.

2 Experimental

2.1 Materials and Equipment

All chemicals and solvents were purchased from AmBeed USA or Sigma-Aldrich/Merck and used without further purification.

Reflection data of single crystals were collected on either a Bruker D8 Venture 4 K Photon III C28 diffractometer or on a Bruker D8 Quest diffractometer. Both instruments are equipped with a graphite monochromator using a Mo-Kα generator utilizing a wavelength of λ = 0.71073 Å. The data was collected using phi and omega scans at 100 K. COSMO [30] was utilized for multiple hemisphere data collection of the reciprocal space. Bruker SAINT-Plus and XPREP [31] were employed for frame integration and data reduction. SADABS [32] was used for phase correction by using the multi-scan method. SHELXT [33] was used to solve the crystal structures by means of intrinsic phasing. WinGX [34], Olex2 [35] and SHELXL-2018/3 [34] were used for the refinement of the crystal structures. DIAMOND 4.0 software [36] was utilized to generate crystal structure images. In the crystal structure images all thermal ellipsoids are drawn with 50% probability level unless stated otherwise. In all structures, the hydrogen atoms were positioned geometrically and refined using a riding model: C–H aromatic distances are placed at 0.95 Å. The H atom isotropic displacement parameters were fixed at $U_{iso}(H) = 1.2\ U_{eq}(C)$. When appropriate, the hydrogen atoms bound to non-carbon atoms were located and placed according to the Fourier electron difference map.

PXRD patterns were collected on a Bruker D2 Phaser powder X-ray diffractometer at 25 °C, with Cu radiation (λ = 1.54 Å). TEM images were obtained from Philips (FEI) CM100 microscope equipped with a MegaView III digital camera and pictures were analyzed with ZEISS ZEN core V2.6 software for particle size determination. ^{1}H NMR spectra were measured on a 400 MHz Bruker AVANCE III NMR spectrometer (operating at 25 °C) with a 5 mm BBI H-BB-D probe with z-gradients. The ^{1}H chemical shifts were reported relative to $SiMe_4$ at 0.0 ppm as external standard and utilizing the solvent peak as internal standard where applicable. All insoluble ML-ZIF derivatives were digested in D_2O: D_2SO_4 (9:1) prior to NMR measurements.

All samples were activated prior to porosity analyses by solvent exchange with methanol (3×50 cm^3) and evacuation at 150 °C. Porosity and surface area measurements were performed on a Micromeritics ASAP 2020 Surface Area and Porosity Analyser. Porosity data was analyzed with MicroActive V2.0 for physisorption with nitrogen and carbon dioxide. The Brunauer – Emmett – Teller (BET) surface area was determined using the recently developed BET surface identification (BETSI) software [37]. N_2 adsorption was measured with relative pressure at 77 K and CO_2 adsorption with absolute pressure at 273 and 293 K, respectively, with the warm and cold free space determined separately with helium. T-plot external surface areas and micropore volumes were calculated with the t-plot method of the Microactive programme using the Harkins and Jura thickness equation. Thermal stability tests were performed on a TA TGA5500 analyzer under N_2 atmosphere.

2.2 De Novo Synthesis of Mixed-Linker ZIFs

Mixed-linker (ML) ZIFs were synthesized using a solvothermal method from literature with equal linker ratios (Scheme 1) [17]. For the synthesis of ML-ZIF-7, $Zn(NO_3)0.6H_2O$ (0.9460 g, 3.2 mmol), 2-nitroimidazole (NO_2Im, 0.4523 g, 4.0 mmol) and 2-chloroimidazole (ClIm, 0.4100 g, 4.0 mmol) were separately dissolved in DMF (20 cm^3). The solutions were then mixed in a Teflon reactor. The reactor was sealed and solvothermally heated at 100 °C for 72 h. The reactor was then allowed to cool to room temperature, the formed crystals were separated by centrifugation and washed with DMF (2×100 cm^3). The crystalline product was air-dried overnight to yield light yellow crystals of ML-ZIF-7_{Cl} ($Zn(NO_2Im)_{1.24}(ClIm)_{0.76}$), (0.6007 g, 67%, based on Zn^{2+}). Similarly, ML-ZIF-8_{Br} was synthesized by using 2-bromoimidazole (BrIm, 0.4100 g,

4.0 mmol) in place of ClIm to yield ML-ZIF-8_{Br} crystals with $Zn(NO_2Im)_{1.16}(BrIm)_{0.84}$ composition (0.8260 g, 82%, based on Zn^{2+}).

2.3 SALE Synthesis of ML-ZIFs

Firstly, nano-sized ZIF-108 was synthesized using an adopted procedure from literature giving an average particle size of 69 nm [26]. SALE was performed by suspending nZIF-108 (0.300 g, 1.0 mmol) in DMF (30 cm^3) by an ultrasonic probe for three minutes before transferring it to a Teflon cup (Scheme 2). Subsequently, ClIm (0.318 g, 3.0 mmol) was dissolved in DMF (30 cm^3) and added to the ZIF-108 suspension. The Teflon cup was then sealed in a stainless-steel reactor and heated to 60 °C for 72 h. After cooling, the SALE products were collected by centrifugation, washed with DMF (3 × 100 cm^3), followed by further centrifugation and air dried to yield ZIF-108-Cl (0.2080 g, 69%)). A similar SALE reaction with BrIm (0.456, 3.0 mmol) yielded ZIF-108-Br (0.2069, 69%).

2.4 CO_2-Epoxide Cycloaddition Reaction

The catalytic activity of de novo and SALE synthesized ML-ZIFs with tetrabutylammonium bromide (TBAB) was tested using optimized reaction conditions (120 °C, 17 bar, 0.2 mol %, 0.5 h) for solvent-less CO_2-propylene-oxide (PrO) cycloaddition in a 25 cm^3 Parr reactor with magnetic stirrer (Scheme 3) [38]. PrO (5 cm^3, 72 mmol), ML-ZIF-7 (40.5 mg, 0.144 mmol) and TBAB (46.4 mg, 0.144 mmol), were placed in the sealed reactor with a CO_2 inlet. The reactor was first purged with CO_2 to replace air with CO_2 inside the reactor. The reactor was then charged with 17 bar of CO_2 and heated to 120 °C for 30 min. After cooling the reactor to room temperature, excess gas was vented and the recovered liquid was analysed via ^{1}H NMR.

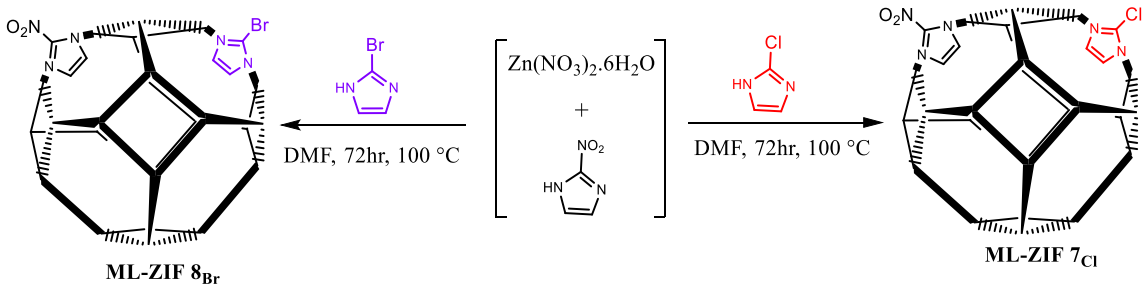

Scheme 1 De novo synthesis of ML-ZIFs

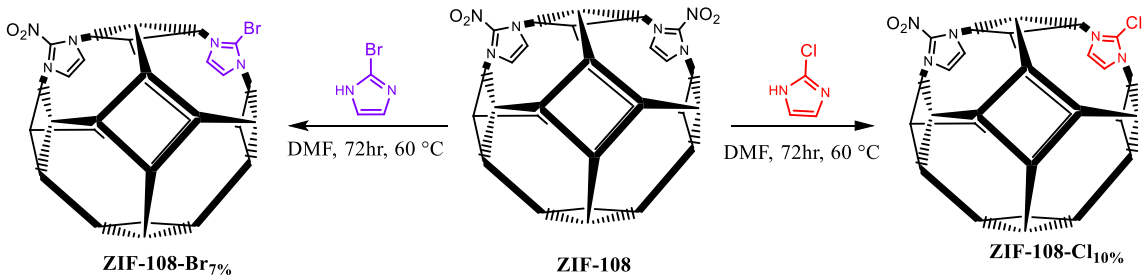

Scheme 2 Summary of SALE synthesis of ML-ZIFs

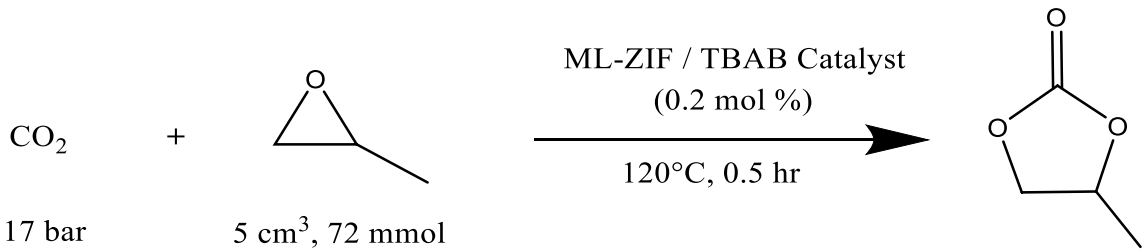

Scheme 3 Cycloaddition of CO_2 to PrO under optimized conditions to afford propylene carbonate

3 Results and Discussions

3.1 Synthesis of Mixed-Linker ZIFs

The mixed linker ZIFs were synthesized with 1:1 linker ratio for the de novo synthesis to afford both linkers an equal chance of incorporation. For the SALE of ZIF-108, 3 × excess secondary linker (ClIm/BrIm) was used as it is adequate for the diffusion-limited ligand exchange process [39, 40]. SALE was performed at 60 °C, as ligand exchange at high temperature result in surface etching of the ZIF [40]. Both de novo and SALE syntheses were performed for 72 h for a synthesis-time independent comparison of the two routes. All ML-ZIF syntheses were performed with a DMF solvent system, as all the linkers (NO_2Im, ClIm and BrIm) used in this work are soluble in DMF, and SALE is dependent on the solubility of the linkers in solution [41].

Thermal gravimetric analyses (TGA) show that the de novo synthesized ML-ZIFs are thermally stable up to 330–340 °C. While ML-ZIFs prepared via SALE are thermally stable up to 300 °C. (Fig. 1) The lower thermal stability of the SALE derivatives can be attributed to the presence of partly coordinated linkers.

3.2 X-Ray Diffraction

3.2.1 Single Crystal XRD

Both products from the de novo syntheses, ML-ZIF-7 and ML-ZIF-8, form a sodalite (SOD) topology with $I\bar{4}3m$ space group, making them isostructures of ZIF-8 and ZIF-108, respectively [17, 42]. The external morphology of the crystals of ML-ZIF-7 and ML-ZIF-8 is given in Fig. 2. The subunit of the two crystal structures is depicted with their respective major and minor disorder occupancies in Fig. 3. The primary disorder occupancies are 0.64 and 0.62 for ML-ZIF-7 and 8, respectively. Each subunit is defined as a whole imidazolate anion with a zinc cation coordinating with each of the aromatic nitrogen atoms of the imidazole. The general crystallographic and refinement parameters for the two crystal structures are given in SI, Table S1. Both crystal structures' unit cell parameters are similar; however, the ML-ZIF-7 structures' unit cell lengths are slightly shorter, resulting in a slightly smaller unit cell volume, and this can be attributed to the larger atomic radius of bromide compared to chloride.

The hexagonal (open pore) and square packing (closed pore) motives of both ML-ZIFs are illustrated in Fig. 4. Some small but significant crystallographic bonding distances and angle differences can be observed between ML-ZIF-7, ML-ZIF-8 and other structures found on the Cambridge Structural Database (CSD) [43]. A selection of these distances and angles has been summarised in Table 1.

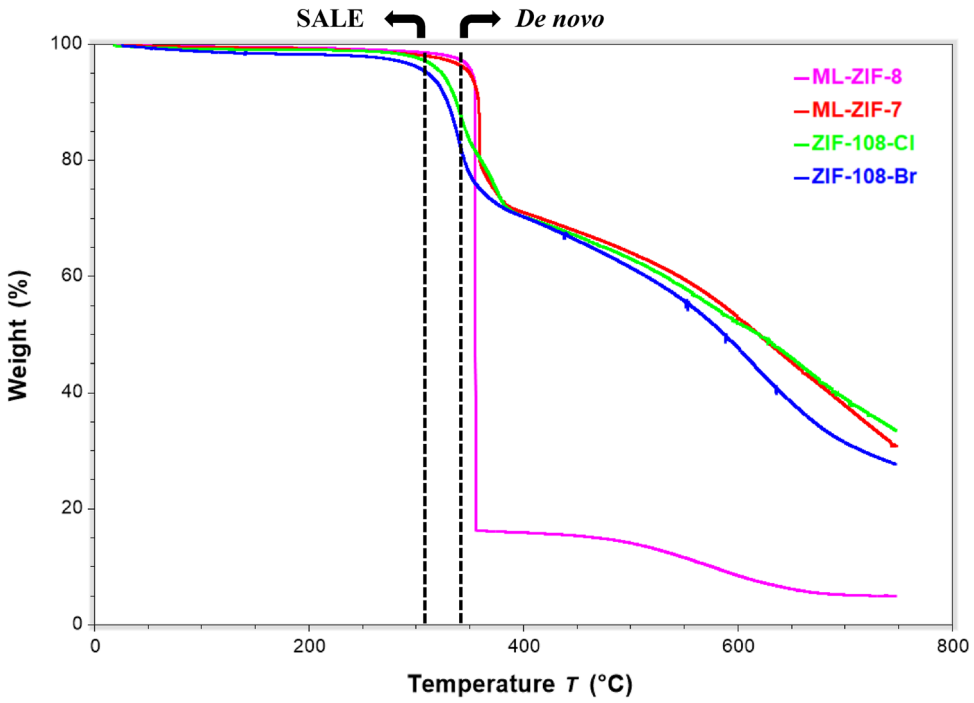

Fig. 1 TGA of ML-ZIFs and ZIF-108 SALE products

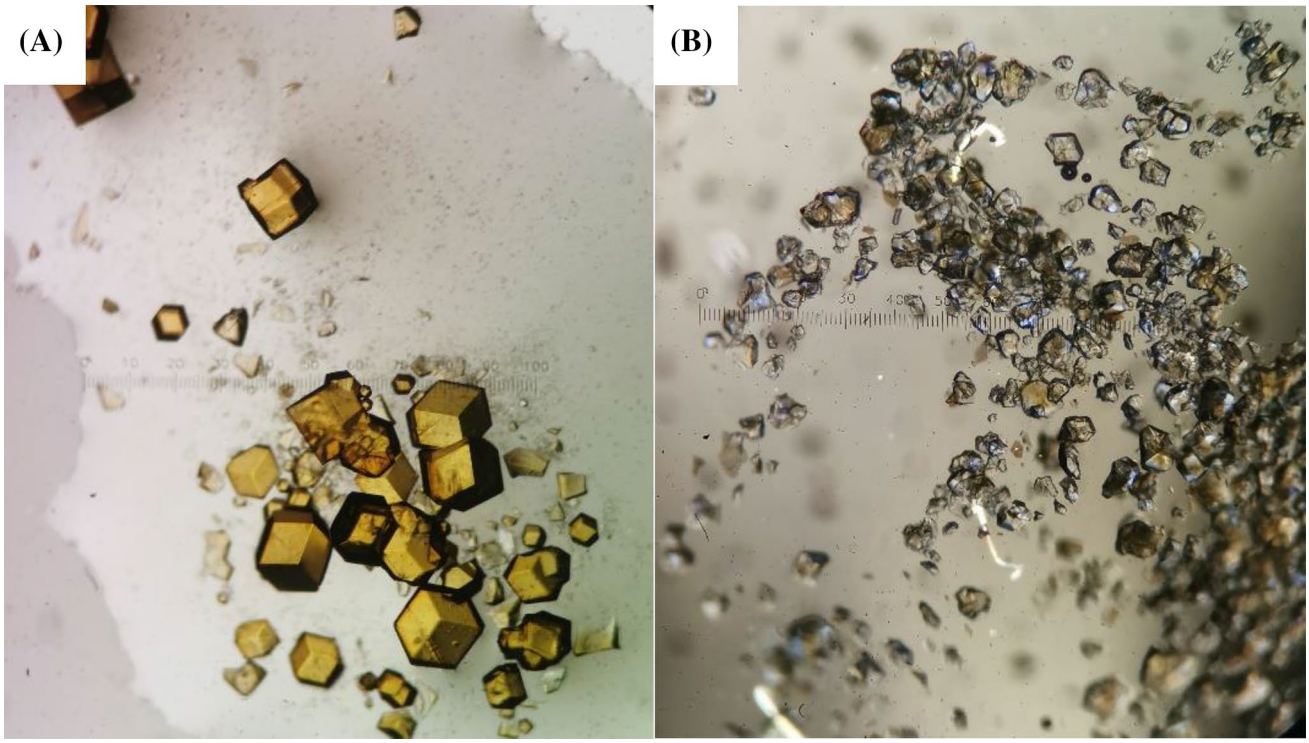

Fig. 2 Crystals of **A** ML-ZIF-7 and **B** ML-ZIF-8 as taken through a polarising microscope with × 45 magnification

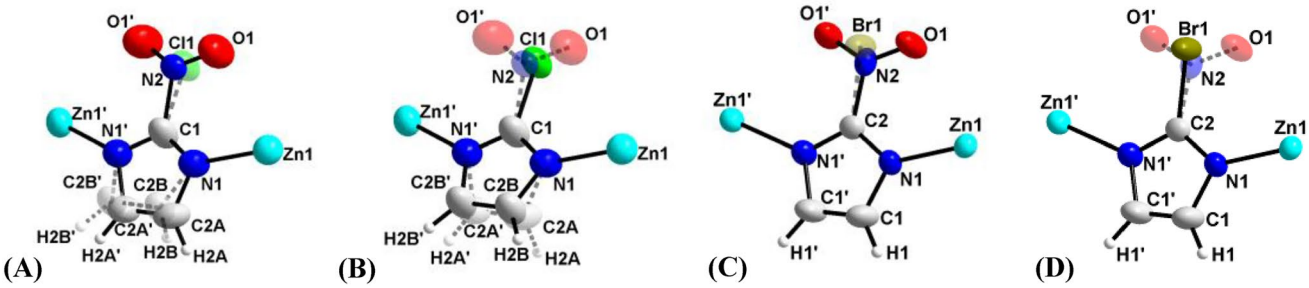

Fig. 3 **A** Subunit of the major (64.0%) and **B** minor occupancies of ML-ZIF-7. **C** Subunit of the major (61.8%) and **D** minor occupancies of ML-ZIF-8

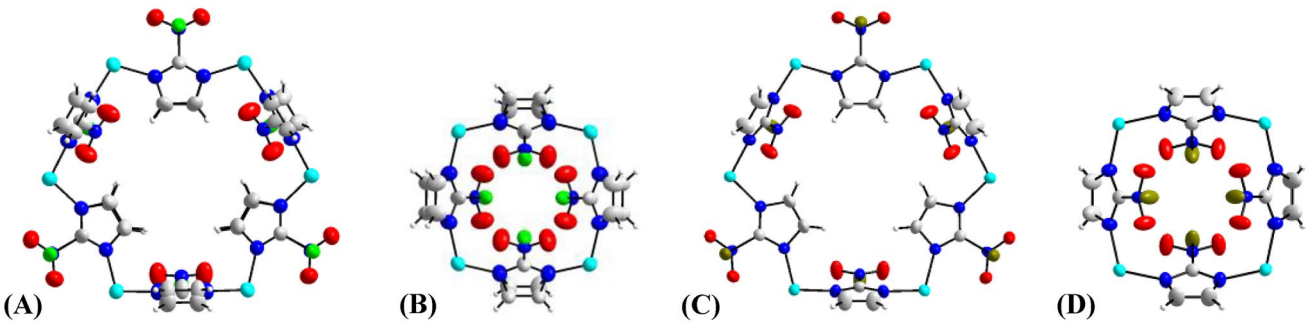

Fig. 4 Hexagonal and square packing units of ML-ZIF-7 (**A**, **B**) and ML-ZIF-8 (**C**, **D**)

Table 1 Selected bonding distances and angles of the structures reported here and of selected structures found in the CSD

Compound	CSD code (Reference)	Distances measurements (Å)			Angle measurements (°)		
		Zn_1-Zn_1'[a]	Zn_1-N_1	Pore diameter[b]	N_1–Zn_1–N_1'	Hexagonal plane angles [c]	Square plane angles[d]
ML-ZIF-7	This work	6.0638(1)	2.007(6)	5.8035(1)	105.9(2)	73.8(9)	63.7(9)
ML-ZIF-8	This work	6.0815(5)	1.999(7)	5.8111(5)	106.5(2)	71.1(8)	69.5(7)
ZIF-8_Cl	YITKIY [44]	6.024(1)	1.942(3)	5.69(2)	108.4(1)	70.3(4)	70.9(4)
ZIF-8_Br	YITKEU [44]	6.039(1)	1.987(4)	5.76(2)	107.6(1)	66.9(5)	77.5(3)
$Zn(Iim)_2$	EJEGUY [45]	6.0777(1)	2.04(2)	5.72(5)	112.5(8)	67.5(1)	76.5(13)
ZIF-108	FOQPAF [46]	6.1135(1)	2.023(1)	5.8812(1)	104.06(5)	73.6(1)	64.3(1)

In cases where a structure on the CSD contained disorders only the major component of the disorder were considered for distance and angle mesurements

[a]The distance separated by an imidazolate bridging ligand

[b]The distance between two directly opposing hydrogen atoms in the hexagonal packing motif

[c]The planes generated through the N_1-Zn_1-N_1' atoms of the two discrete imidazoles in the hexagonal packing motif

[d]The planes generated through the N_1-Zn_1-N_1' atoms of the two discrete imidazoles in the square packing motif

ML-ZIF-7 and ML-ZIF-8 adopt very similar structural parameters to ZIF-108, with some variations being introduced by the presence of Br/Cl atoms. The Zn_1-Zn_1' distance for ZIF-108 (6.1135(1) Å) is longer than those of ML-ZIF-7 and ML-ZIF-8 (6.0638(1) and 6.0815(5) Å), respectively. A similar trend in the Zn_1-Zn_1' distance is observed with the structures of ZIF-8_Cl and ZIF-8_Br being 6.024(1) and 6.039(1) Å. The Zn_1-N_1 distance of ML-ZIF-7 and ML-ZIF-8 are 2.007(6) and 1.999(7) Å which tends toward the value seen in ZIF-108 of 2.023(1) Å and not the shorter distances of ZIF-8_Cl and ZIF-8_Br (1.942(3) and 1.987(4) Å), respectively. The pore diameters of ML-ZIF-7 and ML-ZIF-8 (5.8035(1) and 5.8111(5) Å) are slightly smaller than ZIF-108 (5.8812(1) Å) but are significantly larger than any of the other structures found in 1 (between 5.5502(1) and 5.76(2) Å).

As with the bonding distances, the two structures reported here have angles that mimic those of ZIF-108. The N_1-Zn_1-N_1' angle for ML-ZIF-7 and 8 are 105.9(2) and 106.5(2) °, respectively, whereas ZIF-108's angle is 104.06(5)°. This is smaller than ZIF-8_Cl and ZIF-8_Br angles that are 108.4(1) and 107.6(1) °. The hexagonal and square plane angles show the same trend. For ML-ZIF-7 the hexagonal (73.8(9) °) and square (63.7(9) °) plane angles are identical, within error margins, to ZIF-108's plane angles (73.6(1) and 64.3(1) °). However, ML-ZIF-8's plane angles (71.1(8) and 69.5(7) °) deviate from this, possibly due to the larger bromide atomic radii. The effect of the nuclear radii can be seen in the angles of ZIF-8_Cl, ZIF-8_Br and $Zn(I_2)$, which decrease in the hexagonal plane angles (70.3(4), 66.9(5) and 67.5(1) °) and increase in the square plane angles (70.9(4), 77.5(3) and 76.5(13) °).

These parameters show that the electron-withdrawing NO_2 group is useful in increasing the pore size of chloride and bromide-containing ZIFs, while retaining some differences in electronic character (compared to NO_2 only), which could be useful for gas adsorption.

The unit cell packing of the ML-ZIF-7 and ML-ZIF-8 structures are very similar, as expected, both with SOD topology. In the figure below (Fig. 5) the unit cell packing of both the crystal structures are depicted as line drawings for the sake of clarity. The open hexagonal pores are situated at the corners of the unit cell and the closed square pores are parallel to the faces of the unit cell. Also included in the figure is the polyhedra of the metal cations. These tetragonal-polyhedra are generated by the N-atoms of the imidazolate ligands coordinated to each Zn-cation to highlight the metal positions.

3.2.2 Powder XRD

Directly synthesized ML-ZIFs formed a SOD topology, in agreement with the result obtained from single crystal XRD. (Fig. 6) The ligand exchanged ZIF-108 derivatives retained the SOD topology of ZIF-108. Peak broadening is only observed with the PXRD pattern of SALE products, indicating that the particles are nano-sized.

After activation, the de novo synthesized ML-ZIFs maintained the SOD topology, whereas the ZIF-108 SALE derivatives undergoes a phase change to an unknown, disordered structure. (Fig. 7) The disorder is characterized by a shift of the 110 peak from 7.2° to 6.5° and a significant broadening of all peaks. The phase change has previously been attributed to a strong interaction of the ZIF with methanol during the activation process resulting in amorphization of

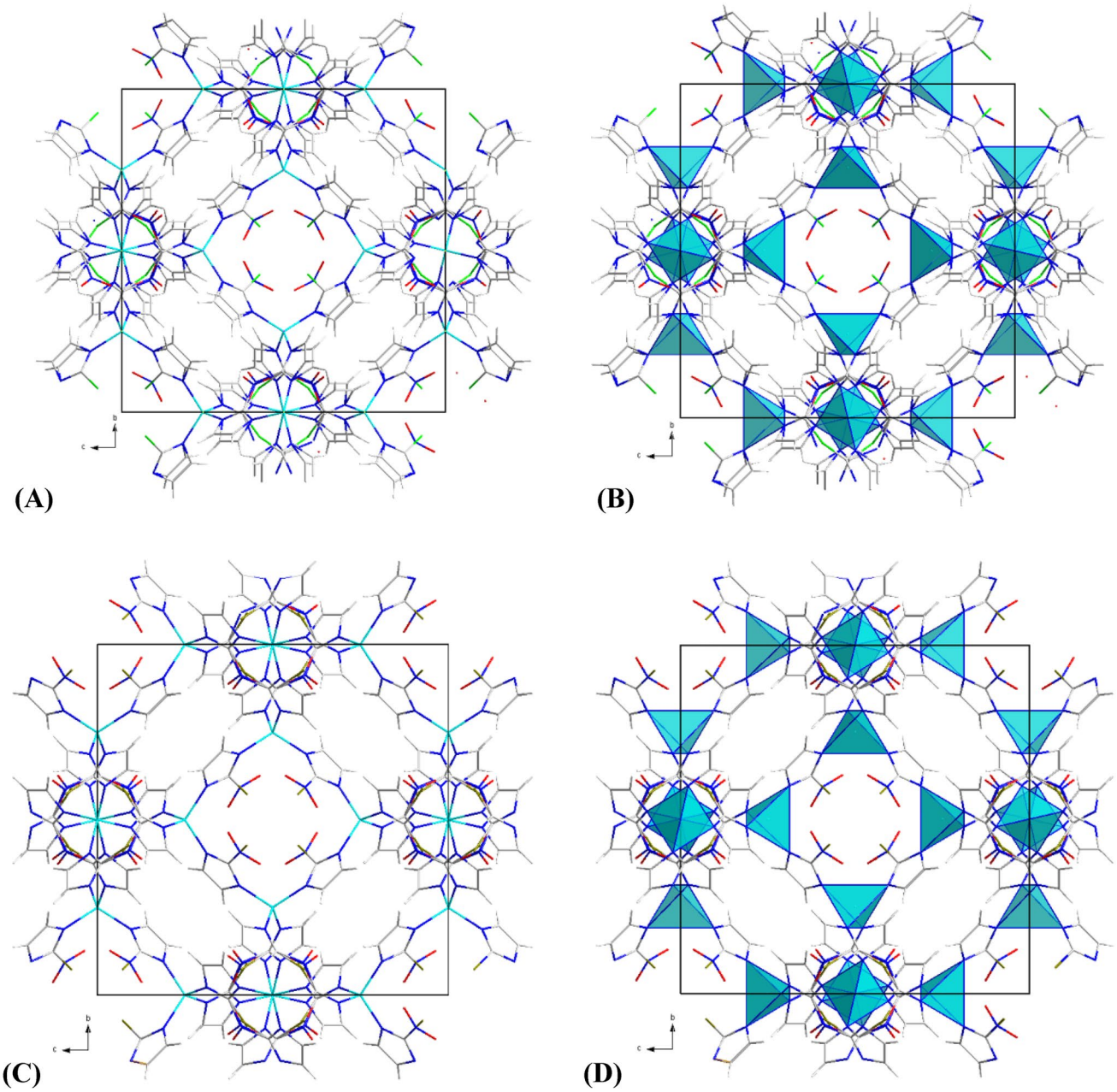

Fig. 5 Unit cell packing of ML-ZIF-7 and ML-ZIF-8 are illustrated as line drawings in (**A**) and (**C**), respectively (as viewed along the *a*-axis). To their right are the same packing with the polyhedra of the Zn coordination sphere **B** for ML-ZIF-7 and **D** for ML-ZIF-8; viewed from the *a*-axis

the structure [29]. These structural instabilities are inherent to the parent ZIF-108, which undergoes a similar structural change in polar solvents and above 100 °C [47]. Similar to ZIF-108, the SOD topology of the SALE products can be restored by immersing them in DMF. (SI, Fig.S1).

3.3 Nuclear Magnetic Resonance (NMR)

After digestive ^{1}H NMR, ML-ZIFs linker ratio was determined from the CH=CH peak integrals of NO_2Im (Fig. 8i) and halogenated imidazoles, respectively. (Fig. 8, i–iii) Directly synthesized ML-ZIFs showed a ~ 60: 40 (NO_2Im: XIm) linker ratio. These results are in line with the occupancy of the two linkers observed with single-crystal XRD. The higher incorporation of the NO_2Im linker in both

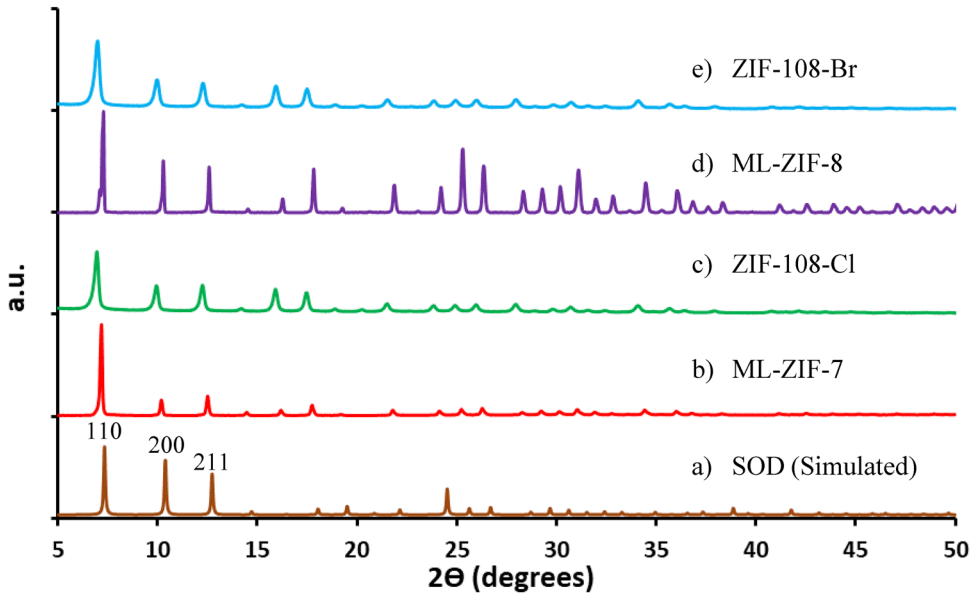

Fig. 6 PXRD pattern of as synthesized mixed-linker ZIFs

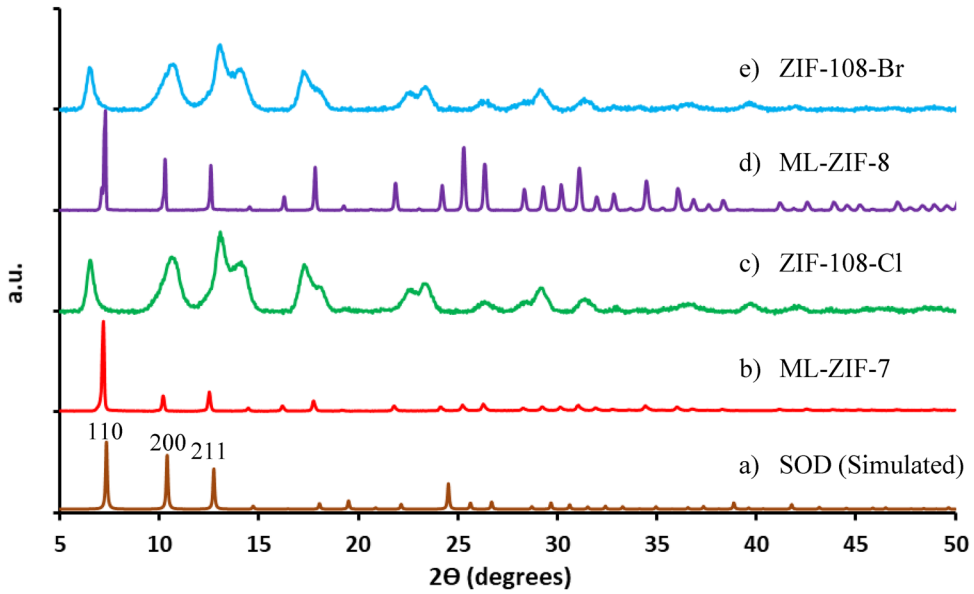

Fig. 7 PXRD pattern of mixed-linker ZIFs after activation

ML-ZIFs can be attributed to the higher reactivity of NO_2Im and favourable ZIF structure formed with NO_2Im over the halogenated linkers [26]. The two SALE products showed low ($\leq 10\%$) incorporation of the halogenated linker. This can be attributed to the exchange being limited to the external surface of ZIF-108, due to the bulkier halogen functionality and steric effect between the -NO_2 and incoming –Cl/Br functionality [48].

3.4 Transmission Electron Microscopy

TEM images of the ML-ZIFs and SALE products revealed the hexagonal and spherical particles, with average particle sizes of 450–480 nm for the de novo prepared ML-ZIFs and 108–125 nm for SALE products. (Fig. 9) Both SALE products showed a significant increase on the size of ZIF-108 (69 nm), indicating a possible core–shell structure, where SALE predominantly occur on the external surface area of the MOF [40]. The SALE synthesis method resulted in nano-sized particles (Fig. 9 C and D), with both de novo syntheses resulting in particles about five times larger (Fig. 9 A and B). This can be ascribed to the particle size of SALE products being limited by the mother ZIF-108, compared to the de novo products, where there is no limiting agent.

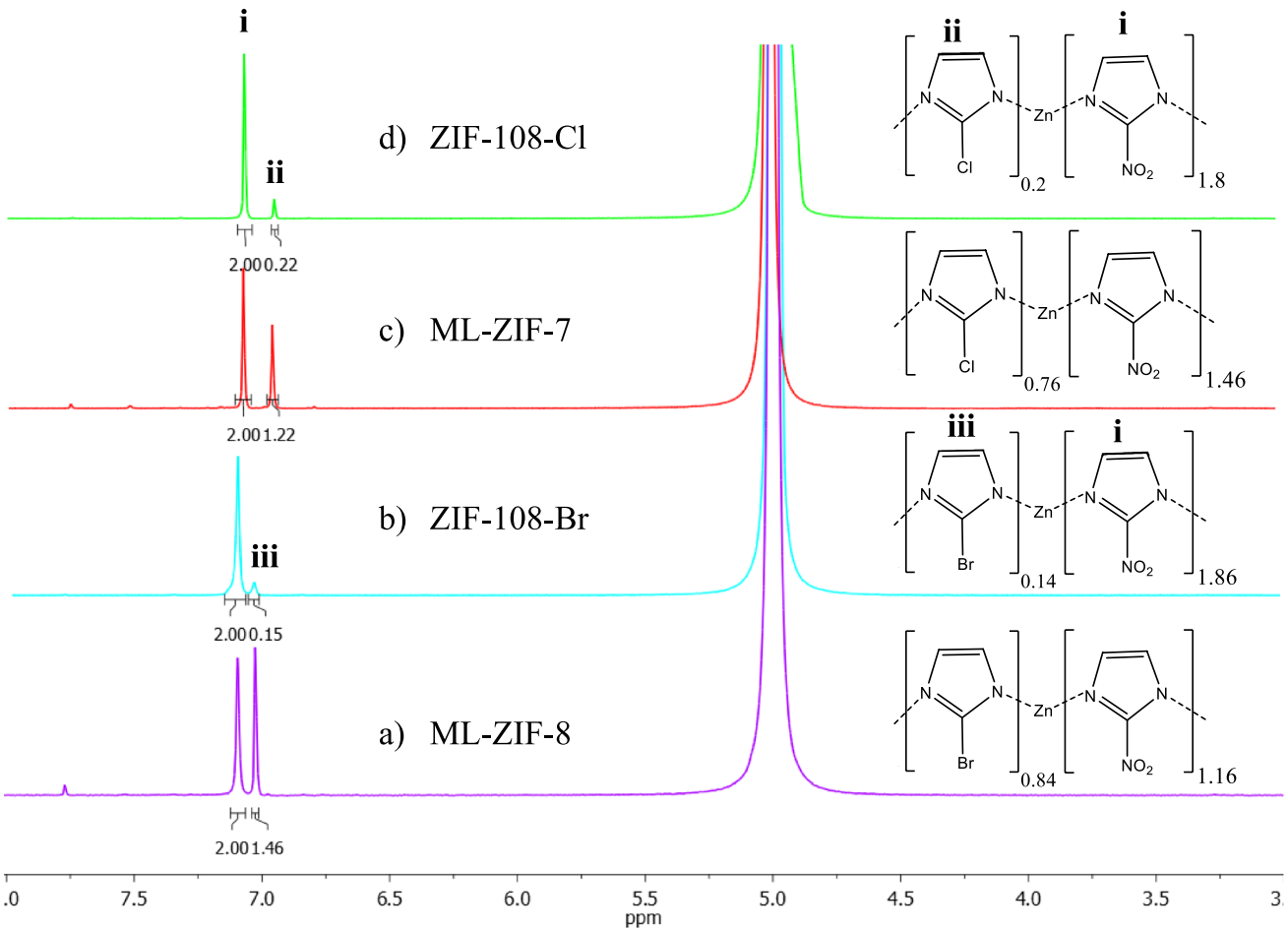

Fig. 8 Digestive ^{1}H NMR of ML-ZIFs and ZIF-108 SALE products

3.5 Porosity Analysis

Both de novo prepared ML-ZIFs and SALE products (from ZIF-108) have a type-I N_2 isotherms. (Fig. 10) In comparison to the reported BET surface area of ZIF-108 (724 m^2 g^{-1}), both ML-ZIFs show significantly larger surface areas, with a 77% (ML-ZIF-7_{Cl}) and 44% (ML-ZIF-8_{Br}) increase [26]. Of the de novo prepared ZIFs, ML-ZIF-7_{Cl} exhibited the highest BET surface area (1283 m^2 g^{-1}) and micropore volume of 0.43 cm^3 g^{-1}. (Table 2, SI Fig. S2–S5) Both de novo prepared ML-ZIFs show superior BET surface areas, compared to their SALE derived analogues (ZIF-108-Cl and ZIF-108-Br) [44].

The ZIF-108 SALE derivatives both have lower BET surface areas than the mother ZIF-108, with a 60 and 47% decrease for ZIF-108-Cl and ZIF-108-Br, respectively (Fig. 10A). This can be attributed to the phase change of the ZIF-108 derivatives during the activation process, as observed in Fig. 8. Noticeable hysteresis is observed with the desorption cycle of ZIF-108_Cl, possibly due to the presence of mesoporous cavities, resulting from the phase change during activation.

The gate opening phenomenon refers to the distortion of the MOF structure at a specific gate opening pressure, resulting in a flexible structure capable of greater molecular uptake [49, 50]. This can be observed in the N_2 isotherm with logarithmically-scaled relative pressure (p/p°) on the x-axis, with each step or "jump" in adsorption corresponding to the gate-opening/flexibility pressure [51]. The N_2 isotherm of ML-ZIF-7_{Cl} exhibits a sharp step (at 0.0005–0.005 p/p°), indicating the flexibility of the framework (Fig. 10B). Similarly, ML-ZIF-8_{Br} also shows a slight step (0.04–0.05 p/p°) at higher loading, resulting in a hysteresis loop in the desorption cycle. Chaplais et al. have demonstrated the gate-opening phenomenon for ZIF-Cl ($Zn(ClIm)_2$), while ZIF-Br ($Zn(BrIm)_2$) showed no flexibility [44, 52]. Therefore, the flexibility of ML-ZIF-7_{Cl} can be attributed to the possible swing/rotation of both the ClIm and NO_2Im linkers, while the slight flexibility of ML-ZIF-8_{Br} can be ascribed to the NO_2Im linker rather than the BrIm linker.

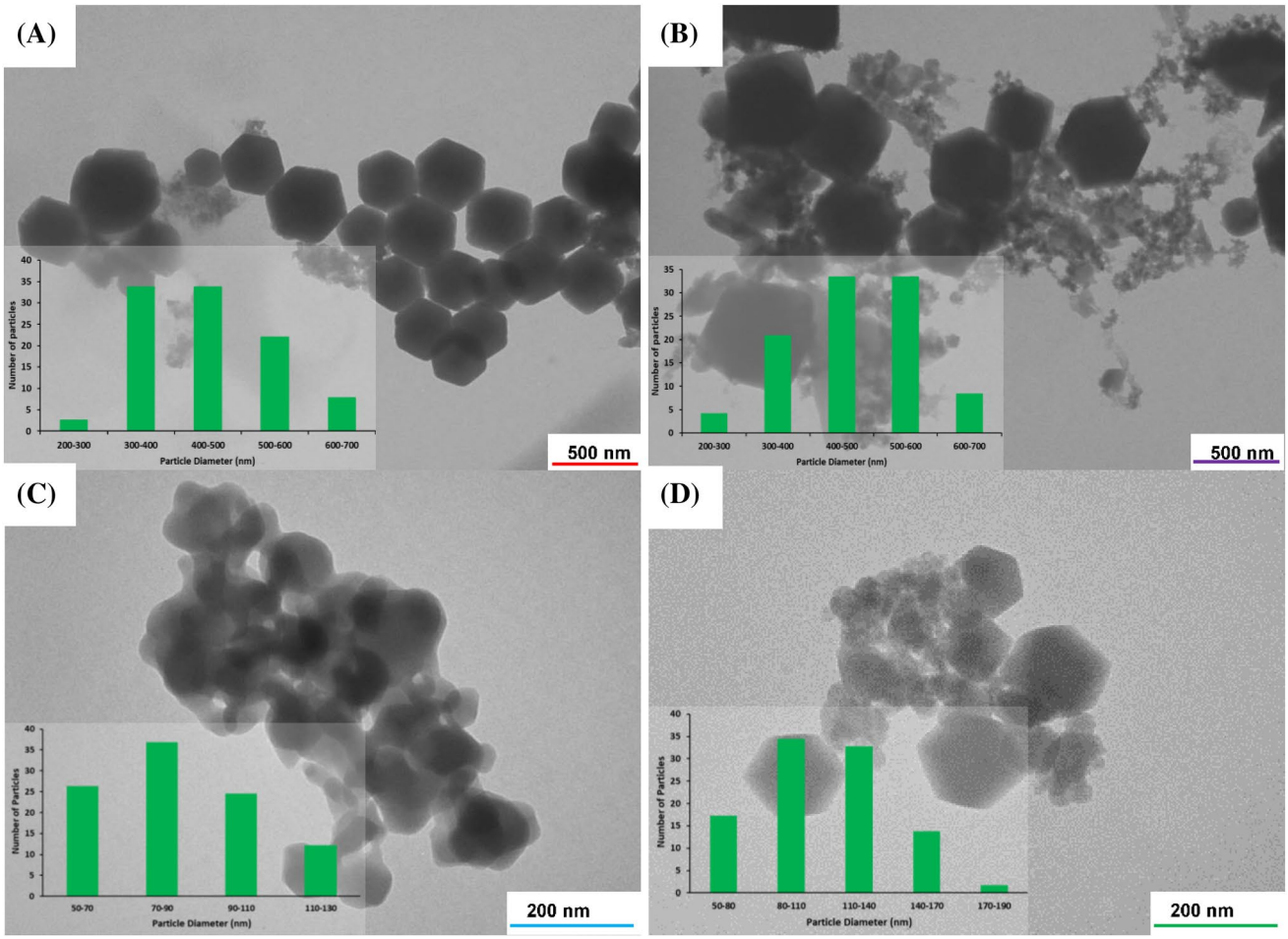

Fig. 9 TEM images and particle size distribution of **A** ML-ZIF-7_{Cl}, **B** ML-ZIF-8_{Br}, **C** ZIF-108-Cl and **D** ZIF-108-Br

3.6 CO_2 Adsorption

At low pressures (0–200 mmHg) SALE synthesized ML-ZIFs show similar CO_2 uptakes than de novo ML-ZIFs. (Fig. 11) At higher pressures (200–900 mmHg) the de novo prepared ML-ZIFs maintain a linear increase while the SALE derivatives level off due to their lower porosities. ML-ZIF-8_{Br} and ML-ZIF-7_{Cl} have 60 and 70% higher CO_2 uptakes than the 53 $cm^3\ g^{-1}$ of ZIF-108 (Table 2). The 90 $cm^3\ g^{-1}$ CO_2 uptake of ML-ZIF-7_{Cl} can be attributed to its higher porosity and gate-opening effect. At a higher analysis temperature (293 K), both de novo prepared ML-ZIFs show similar uptakes. (SI, Fig. S6).

The CO_2 uptakes of the SALE derived ML-ZIFs, ZIF-108-Br (50 $cm^3\ g^{-1}$) and ZIF-108-Cl (55 $cm^3\ g^{-1}$), are similar to that of ZIF-108 (53 $cm^3\ g^{-1}$), despite their lower BET surface and phase change during activation (Table 2).This highlights the effect of the lowly incorporated halogenated linkers in enhancing the CO_2 uptake. The higher CO_2 uptake of the Cl-containing ML-ZIF-7_{Cl} and ZIF-108-Cl, when compared to their Br-containing counterparts, is in line with the computational studies done by Tsai et al., which showed that –Cl functionalised ZIFs result in stable adsorption energies over other halogen functionalities [53].

3.7 CO_2 Conversion via Cycloaddition Reactions

While CO_2 is known to be a major contributor to global warming, it is also considered as a renewable, non-toxic, and abundant feedstock for fine chemical production [54]. However, due to its high kinetic and thermodynamic stability, converting CO_2 into useful chemicals requires significant energy input [55]. One promising approach to overcome this challenge is through the catalytic fixation of CO_2 into cyclic carbonates, which are versatile chemicals with a range of applications, including use as intermediates, polar aprotic solvents, polymers, electrolytes, and

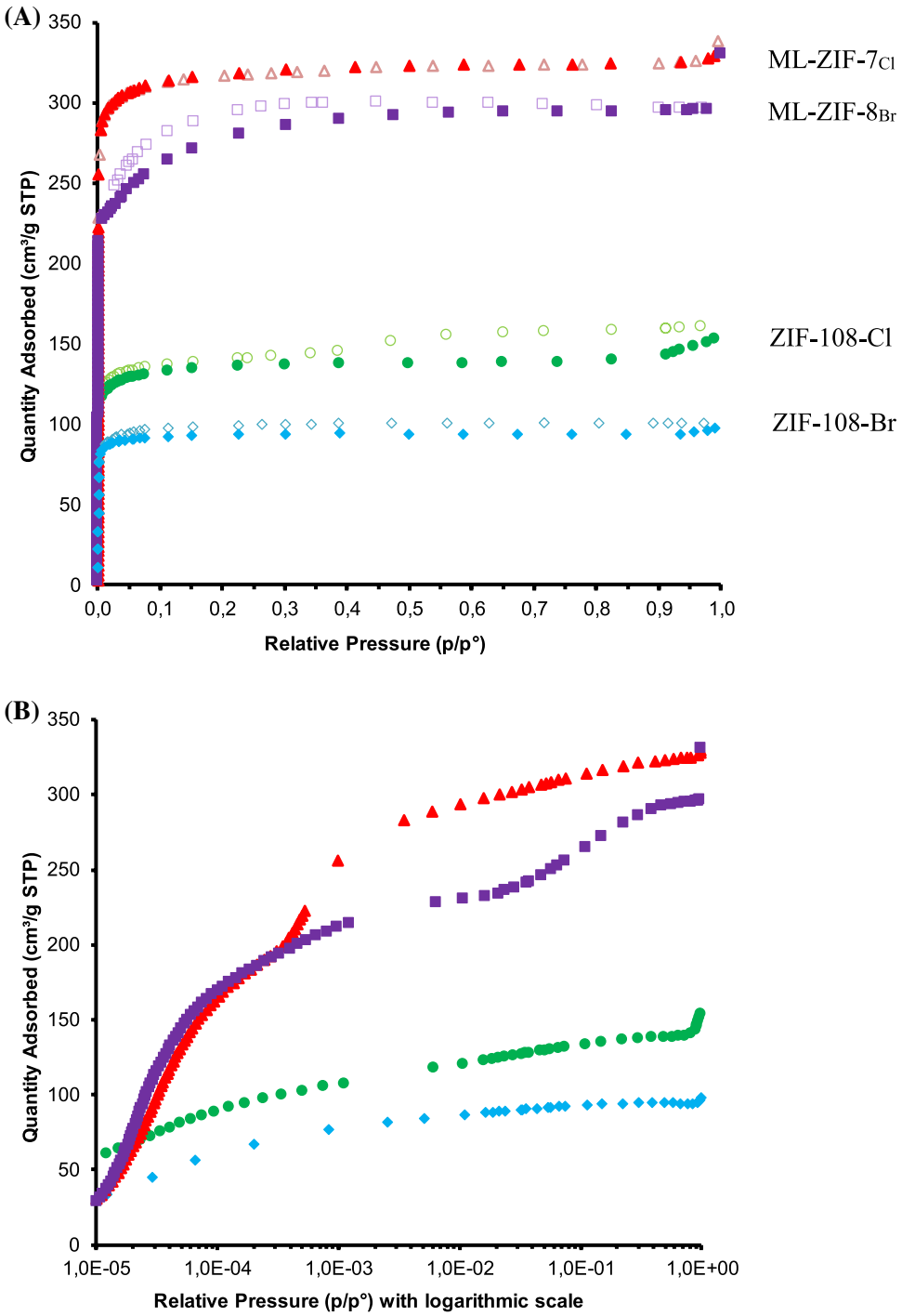

Fig. 10 N_2 isotherms of ML-ZIFs at 77 K **A** with linear scale and **B** with logarithmic scale of the relative pressure}: ML-ZIF-8_{Br} (purple, ■), ML-ZIF-7_{Cl} (red,▲), ZIF-108-Cl (green, ●), and ZIF-108-Br (blue,◆). Adsorption are marked by solid and desorption by hollow symbols (Color figure online)

Table 2 Porosity analyses and CO_2 uptake of mixed-linker ZIFs

Name	Linker ratio NO_2Im: Cl/Br Im	N_2 adsorption at 0.8 p/po (cm^3g^{-1})		BET (m^2g^{-1})	Micropore Volume (cm^3g^{-1})	CO_2 uptake At 273 K (cm^3g^{-1})
ZIF-108-Cl	1.8: 0.2	140	539		0.18	55
ZIF-108-Br	1.86: 0.14	94	384		0.13	50
ML-ZIF-7_{Cl}	1.24: 0.76	324	1287		0.43	90
ML-ZIF-8_{Br}	1.16: 0.84	294	1037		0.37	85

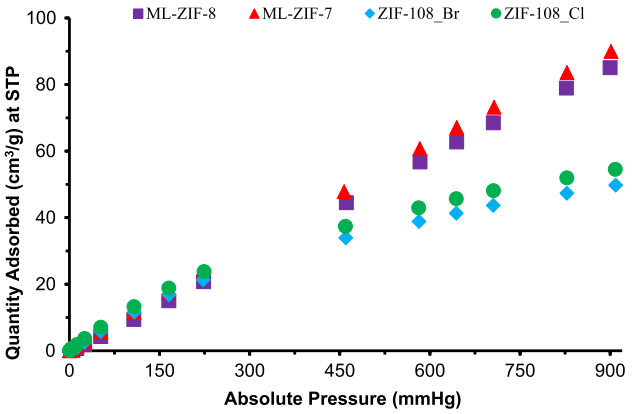

Fig. 11 CO_2 adsorption isotherms of ML-ZIFs and ZIF-108 SALE products at 273 K

Table 3 Cycloaddition of CO_2 with PrO using ML-ZIF and ZIF-108 SALE products as catalyst, with optimized catalytic conditions (0.2/120 °C /17 bar/0.5 h)

Catalyst	Conversion (%)	Selectivity (%)	TON	TOF (h^{-1})
ML-ZIF-7	1	95	5	10
ML-ZIF-8	1	95	5	10
ZIF-108-Cl	–	–	–	–
ZIF-108-Br	–	–	–	–
TBAB	64	95	160	320
ML-ZIF-7/TBAB	89	95	223	446
ML-ZIF-8/TBAB	86	95	215	431
ZIF-108-Cl/TBAB	86	95	215	431
ZIF-108-Br/TBAB	82	95	205	410

fuel additives. Currently, cyclic carbonates are synthesized through either transesterification of diols using toxic solvents or cycloaddition of epoxide substrates with CO_2 [9, 56]. ZIFs, due to their stability, ease of separation, and recyclability, are considered as effective heterogeneous catalysts for CO_2-epoxide cycloaddition [11, 12].

The catalytic activity of de novo and SALE synthesized ML-ZIFs for the PrO-CO_2 cycloaddition reaction (Scheme 3) was tested using optimized reaction conditions (Table 3) [27]. De novo synthesised ML-ZIFs show very low catalytic activity for PrO-CO_2 cycloaddition, while the ZIF-108 derivatives show no catalytic activity at all. The inactivity of the ML-ZIFs can be attributed to the weakening of LB sites (imidazolate linkers) due to the high electronegativity of $–NO_2$, and –Cl/–Br functionalities [57, 58]. Thus, upon addition of a Lewis base co-catalyst, tetrabutylammonium bromide (TBAB), the catalytic activities of the ML-ZIFs were hugely enhanced [59, 60].

Combining TBAB with the ML-ZIFs resulted in a minimum 28% increase in the catalytic activity of TBAB on its own. This can be attributed to the high surface area and CO_2 capacity of the ML-ZIFs, enhancing the interaction of CO_2 with the epoxide substrates. In line with its higher BET surface area and CO_2 uptake, ML-ZIF-7/TBAB resulted in the highest catalytic activity, with Turnover Frequency (TOF) of 446 h^{-1}. The combination of SALE products (ZIF-108-Cl and ZIF-108-Br) with TBAB result in slightly lower activity than for the de novo ML-ZIFs, while the selectivity was maintained.

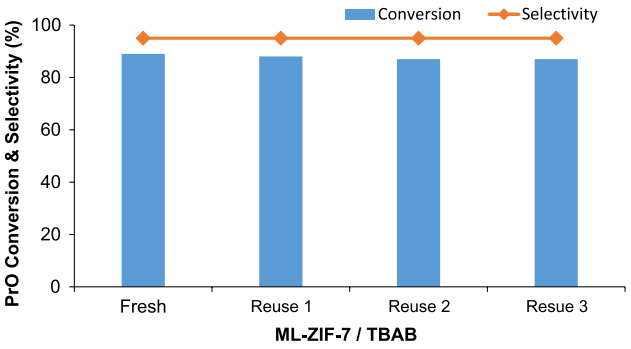

Fig. 12 Catalyst reusability of ML-ZIF-7/TBAB for PrO-CO_2 cycloaddition

Table 4 Catalytic activity of ML-ZIF-7/TBAB on various epoxide substrates

Epoxide	Conversion (%)	Selectivity (%)	TOF (h^{-1})
Propylene Oxide	89	95	446
Epichlorohydrin	79	95	394
1,2-Epoxybutane	89	95	446
Limonene-1,2-epoxide	2	95	10

3.7.1 Catalyst Reusability

The reusability of the high-performing ML-ZIF-7/TBAB catalyst combination was evaluated by isolating and reactivating the catalyst using centrifugation, washing with dichloromethane (DCM) and drying at 60 °C. The ML-ZIF-7/TBAB catalyst combination is reusable for up to four cycles with a slight drop in activity, while the selectivity remained at 95% (Fig. 12). FTIR analyses show that both fresh and recovered catalyst (after 3rd reuse) have similar peaks, confirming the chemical integrity of the catalyst during the reuse (SI, Fig. S7). The slight decrease in catalytic activity can be attributed to the catalyst's mass loss (< 5%). The SALE product, ZIF-108-Cl, on the other hand, undergoes significant degradation during the cycloaddition reaction, and no catalyst could be recovered for reusability tests.

Table 5 Comparison of ML-ZIF 7/ TBAB with reported ZIF derivatives for CO_2-PrO Cycloaddition

Catalyst	Catalytic conditions mole%/T/P_{CO2}/time	Co-catalyst	Reuse (cycles)	TOF* (h^{-1})	References
ZIF-67	0.56/120 °C/10 bar/6 h	–	–	33	[62]
ZIF-22	0.2/120 °C/12 bar/2 h	–	–	237	[12]
ZIF-23	1.8/120 °C/12 bar/6 h	–	≥3	8	[60]
ZIF-90	0.18/120 °C/12 bar/6 h	–	–	17	[63]
F-ZIF-90	0.18/120 °C/12 bar/6 h	–	0	83	[63]
ZIF-90-IL-1	1/90 °C/12 bar /8 h	–	≥3	12	[11]
ZIF-95/TBAB	0.4/80 °C/12 bar /2 h	TBAB	≥5	104	[59]
ZIF-71	0.2/120 °C/12 bar /4 h	–	≥5	124	[64]
ML-ZIF-4	0.2/120 °C/15 bar/0.5 h	–	0	806	[27]
ML-ZIF 5_{Co}	0.2/120 °C/17 bar/0.5 h	–	2	892	[38]
ML-ZIF 7/TBAB	0.2/ 120 °C/17 bar/0.5 h	TBAB	≥4	446	*

*This work

3.7.2 Versatility of ML-ZIF-7/TBAB Catalyst

The versatility of the ML-ZIF-7/TBAB catalyst was tested for the fixation of CO_2 with various functionalized epoxide substrates. (Table 4) ML-ZIF-7/TBAB show good conversion of terminal epoxides with the higher TOF (446 h^{-1}) attained from the conversion of epoxides with electron-donating functional groups (H, CH_3). Low activity was observed for bulky epoxides fixation due to the epoxide's steric hindrance [61].

3.7.3 Comparison with Other ZIF Catalyst

Compared to previously reported ZIF-based catalysts for CO_2-PrO cycloaddition, the catalytic activity (in terms of TOF) of ML-ZIF-7_{Cl}/TBAB ranks only behind that of ML-ZIF-4 and ML-ZIF-5_{Co}, as shown in Table 5. However, while the latter two catalysts demonstrate high activity, they are not reusable beyond two cycles due to significant structural decomposition during the catalytic reaction. In contrast, ML-ZIF-7_{Cl}/TBAB is capable of being reused for up to four cycles while maintaining its chemical integrity, making it an ideal choice for high-scale industrial applications.

4 Conclusions

By using either De novo synthesis and SALE synthesis a combination of NO_2Im and ClIm or BrIm linkers could be successfully incorporated in the ML-ZIF structure. Both methods resulted in ML-ZIFs with SOD topology. The de novo synthesis method is efficient in forming a mixed linker distribution with high chemical (in polar solvents) and thermal stability (up to 340 °C). The core- (–NO_2 functionalized) shell (–Cl/ –Br functionalized) structured SALE products showed low incorporation of the halogenated linker, about 60% increase on the ZIF-108 particle size and phase change during activation.

De novo synthesized ML-ZIFs showed higher porosity and larger particle sizes (~450 nm) than the ZIF-108 derivative SALE products. The chlorinated ML-ZIF-7_{Cl} formed a flexible framework with a structural rotation at 0.0005–0.005 p/p0 of N_2 adsorption. ML-ZIFs with ClIm linkers resulted in higher CO_2 adsorption and fixation than their corresponding BrIm containing ML-ZIFs, in line with their high porosity, electronegativity, and flexibility.

Both de novo and SALE synthesised ML-ZIFs on their own showed no catalytic activities for the fixation of CO_2 with PrO. However, in combination with TBAB co-catalyst, a 28–40% increase in the catalytic activity of TBAB was achieved. ML-ZIF-7/TBAB resulted in the highest activity for CO_2-PrO cycloaddition with a TOF of 446 h^{-1} and 95% selectivity. The catalyst combination was reusable for up to 4 cycles with a slight loss in activity and was versatile for the fixation of CO_2 with various functionalised terminal epoxide substrates.

Supplementary Information The online version contains supplementary material available at https://doi.org/10.1007/s10904-023-02653-5.

Acknowledgements This work was financially supported by the National Research Foundation of South Africa (Grant Number: 121540 for Y.W. Abraha) and a SASOL University Collaboration Grant for E.H.G. Langner. The authors acknowledge the Inorganic Chemistry Section (UFS) for single-crystal XRD analyses, iThemba labs for PXRD analyses, and the Centre of Microscopy (UFS) for TEM images.

Author Contributions YWA: Data curation, Formal analysis, Writing—original draft, Writing—review & editing, Conceptualization. FJFJ: Data curation, Formal analysis Writing—original draft. AB: Writing—review & editing, Resources. EHGL: Writing—review & editing, Supervision, Project administration, Resources, Funding acquisition.

Funding Open access funding provided by University of the Free State. This work was funded by the National Research Foundation of South

Africa (Grant Number: 121540 for Y.W. Abraha) and a SASOL University Collaboration Grant for E.H.G. Langner.

Data Availability The datasets generated during and/or analysed during the current study are available from the corresponding author on reasonable request.

Declarations

Conflict of interest The authors have no relevant financial or non-financial interests to disclose.

References

1. Y.S. Bae, R.Q. Snurr, Development and evaluation of porous materials for carbon dioxide separation and capture. Angew. Chem. Int. Ed. **50**, 11586–11596 (2011). https://doi.org/10.1002/anie.201101891
2. S.D. Kenarsari, D. Yang, G. Jiang, S. Zhang, J. Wang, A.G. Russell, Q. Wei, M. Fan, Review of recent advances in carbon dioxide separation and capture. RSC Adv. **3**, 22739–22773 (2013). https://doi.org/10.1039/c3ra43965h
3. H.N. Abdelhamid, Removal of carbon dioxide using zeolitic imidazolate frameworks: adsorption and conversion via catalysis. Appl. Organomet. Chem. (2022). https://doi.org/10.1002/AOC.6753
4. M. Ding, R.W. Flaig, H.L. Jiang, O.M. Yaghi, Carbon capture and conversion using metal-organic frameworks and MOF-based materials. Chem. Soc. Rev. **48**, 2783–2828 (2019). https://doi.org/10.1039/c8cs00829a
5. K.S. Park, Z. Ni, A.P. Cote, J.Y. Choi, R. Huang, F.J. Uribe-Romo, H.K. Chae, M. O'Keeffe, O.M. Yaghi, ZIFs—first synthesis. Proc. Natl. Acad. Sci. **103**, 10186–10191 (2006). https://doi.org/10.1073/pnas.0602439103
6. B.R. Pimentel, A. Parulkar, E.K. Zhou, N.A. Brunelli, R.P. Lively, Zeolitic imidazolate frameworks: next-generation materials for energy-efficient gas separations. Chemsuschem **7**, 3202–3240 (2014). https://doi.org/10.1002/cssc.201402647
7. V. Masson-Delmotte, P. Zhai, H.-O. Pörtner, D. Roberts, J. Skea, P.R. Shukla, A. Pirani, W. Moufouma-Okia, C. Péan, R. Pidcock, S. Connors, J.B.R. Matthews, Y. Chen, X. Zhou, M.I. Gomis, E. Lonnoy, T. Maycock, M. Tignor, T. Waterfield, IPCC report global warming of 1.5°C, 2018. www.environmentalgraphiti.org.
8. K. Kiatkittipong, M.A.A.M. Shukri, W. Kiatkittipong, J.W. Lim, P.L. Show, M.K. Lam, S. Assabumrungrat, Green pathway in utilizing CO_2 via cycloaddition reaction with epoxide-a mini review. Processes (2020). https://doi.org/10.3390/PR8050548
9. M.H. Beyzavi, C.J. Stephenson, Y. Liu, O. Karagiaridi, J.T. Hupp, O.K. Farha, Metal-organic framework-based catalysts: chemical fixation of CO_2 with epoxides leading to cyclic organic carbonates. Front. Energy Res. **3**, 1–10 (2015). https://doi.org/10.3389/fenrg.2014.00063
10. M. Ding, S. Chen, X.Q. Liu, L.B. Sun, J. Lu, H.L. Jiang, Metal-organic framework-templated catalyst: synergy in multiple sites for catalytic CO_2 fixation. Chemsuschem **10**, 1898–1903 (2017). https://doi.org/10.1002/cssc.201700245
11. H. Yuan, Y. Wu, X. Pan, L. Gao, G. Xiao, Pyridyl ionic liquid functionalized ZIF-90 for catalytic conversion of CO_2 into cyclic carbonates. Catal. Lett. **150**, 3561–3571 (2020). https://doi.org/10.1007/s10562-020-03259-z
12. G.Y. Hwang, R. Roshan, H.S. Ryu, H.M. Jeong, S. Ravi, M. Kim, D.W. Park, A highly efficient zeolitic imidazolate framework catalyst for the co-catalyst and solvent free synthesis of cyclic carbonates from CO_2. J. CO2 Util. **15**, 123–130 (2016). https://doi.org/10.1016/j.jcou.2016.02.005
13. Y. Liu, J. Liu, M. Chang, C. Zheng, Effect of functionalized linker on CO_2 binding in zeolitic imidazolate frameworks: density functional theory study. J. Phys. Chem. C. **116**, 16985–16991 (2012). https://doi.org/10.1021/jp302619m
14. L.H. Wee, S. Vandenbrande, S.M.J. Rogge, J. Wieme, K. Asselman, E.O. Jardim, J. Silvestre-Albero, J.A.R. Navarro, V. Van Speybroeck, J.A. Martens, C.E.A. Kirschhock, Chlorination of a zeolitic-imidazolate framework tunes packing and van der Waals interaction of carbon dioxide for optimized adsorptive separation. J. Am. Chem. Soc. **143**, 4962–4968 (2021). https://doi.org/10.1021/jacs.0c08942
15. A. Sirjoosingh, S. Alavi, T.K. Woo, Grand-canonical monte carlo and molecular-dynamics simulations of carbon-dioxide and carbon-monoxide adsorption in zeolitic imidazolate framework materials. J. Phys. Chem. C. **114**, 2171–2178 (2010). https://doi.org/10.1021/jp908058n
16. W. Morris, B. Leung, H. Furukawa, O.K.M. Yaghi, N. He, H. Hayashi, Y. Houndonougbo, M. Asta, B.B. Laird, O.K.M. Yaghi, B. Leung, N. He, H. Furukawa, O.K.M. Yaghi, Y. Houndonougbo, N. He, H. Hayashi, Y. Houndonougbo, M. Asta, B.B. Laird, O.K.M. Yaghi, A combined experimental-computational investigation of carbon dioxide capture in a series of isoreticular zeolitic imidazolate frameworks. J. Am. Chem. Soc. **132**, 11006–11008 (2010). https://doi.org/10.1021/ja104035j
17. R. Banerjee, A. Phan, B. Wang, C. Knobler, H. Furukawa, M. O'Keeffe, O.M. Yaghi, High-throughput synthesis of zeolitic imidazolate frameworks and application to CO_2 capture. Science **319**, 939–943 (2008). https://doi.org/10.1126/science.1152516
18. A. Phan, C.J. Doonan, F.J. Uribe-Romo, C.B. Knobler, M.O. O'Keeffe, O.M. Yaghi, Synthesis, structure, and carbon dioxide capture properties of zeolitic imidazolate frameworks. Acc. Chem. Res. **43**, 58–67 (2010). https://doi.org/10.1021/ar900116g
19. B. Wang, H. Furukawa, A.P. Cotre, M. O'Keeffe, O.M. Yaghi, Colossal cages in zeolitic imidazolate frameworks as selective carbon dioxide reservoirs. Nature **453**, 207–211 (2008). https://doi.org/10.1021/ja809459e
20. W. Morris, N. He, K.G. Ray, P. Klonowski, H. Furukawa, I.N. Daniels, Y.A. Houndonougbo, M. Asta, O.M. Yaghi, B.B. Laird, A combined experimental-computational study on the effect of topology on carbon dioxide adsorption in zeolitic imidazolate frameworks. J. Phys. Chem. C. **116**, 24084–24090 (2012). https://doi.org/10.1021/jp307170a
21. L. Hu, Z. Yan, X. Mo, X. Peng, L. Chen, Morphology control synthesis of ZIF-8 as highly efficient catalyst for the cycloaddition of CO2 to cyclic carbonate. ChemCatChem **11**, 3212–3219 (2019). https://doi.org/10.1002/cctc.201900735
22. L. Hu, L. Chen, X. Peng, J. Zhang, X. Mo, Y. Liu, Z. Yan, Bifunctional metal-doped ZIF-8: a highly efficient catalyst for the synthesis of cyclic carbonates from CO_2 cycloaddition. Microporous

Mesoporous Mater. **299**, 110123 (2020). https://doi.org/10.1016/j.micromeso.2020.110123
23. Y.F. Lin, K.W. Huang, B.T. Ko, K.Y.A. Lin, Bifunctional ZIF-78 heterogeneous catalyst with dual Lewis acidic and basic sites for carbon dioxide fixation via cyclic carbonate synthesis. J. CO2 Util. **22**, 178–183 (2017). https://doi.org/10.1016/j.jcou.2017.10.005
24. Y.W. Abraha, C. Tsai, J.W. Hans Niemantsverdriet, E.H.G. Langner, Correction to "optimized CO_2 capture of the zeolitic imidazolate framework ZIF-8 modified by solvent-assisted ligand exchange." ACS Omega. **6**, 26821 (2021). https://doi.org/10.1021/acsomega.1c04545
25. C.W. Tsai, J.W. Niemantsverdriet, E.H.G. Langner, Enhanced CO_2 adsorption in nano-ZIF-8 modified by solvent assisted ligand exchange. Microporous Mesoporous Mater. **262**, 98–105 (2018). https://doi.org/10.1016/j.micromeso.2017.11.024
26. Y. Ban, Y. Li, Y. Peng, H. Jin, W. Jiao, X. Liu, W. Yang, Metal-substituted zeolitic imidazolate framework ZIF-108: gas-sorption and membrane-separation properties. Chem. Eur. J. **20**, 11402–11409 (2014). https://doi.org/10.1002/chem.201402287
27. Y.W. Abraha, C. Tsai, E.H.G. Langner, Scalable synthesis of mixed—linker (Zn) ZIFs and their application in—CO_2 adsorption and fixation. J. Porous Mater. **30**, 149 (2023). https://doi.org/10.1007/s10934-022-01326-x
28. O. Karagiaridi, W. Bury, J.E. Mondloch, J.T. Hupp, O.K. Farha, Solvent-assisted linker exchange: an alternative to the de novo synthesis of unattainable metal-organic frameworks. Angew. Chem. Int. Ed. **53**, 4530–4540 (2014). https://doi.org/10.1002/anie.201306923
29. Y. Ban, Y. Peng, Y. Zhang, H. Jin, A. Guo, W. Jiao, P. Wang, Y. Li, W. Yang, Dual-ligand zeolitic imidazolate framework crystals and oriented films derived from metastable mono-ligand ZIF-108. Microporous Mesoporous Mater. **219**, 190–198 (2016). https://doi.org/10.1016/j.micromeso.2015.08.013
30. U. COSMO, Version 1.48, Bruker AXS Inc., Madison, Wisconsin, COSMO, (2003).
31. Bruker, SAINT-PLUS, Version 7.12 (including XPREP), Bruker AXS Inc., Madison, Wisconsin, USA, (2004).
32. Bruker. SADABS. Bruker AXS Inc., Madison, Wisconsin, USA, (2001).
33. G.M. Sheldrick, SHELXT-Integrated space-group and crystal-structure determination. Acta Crystallogr. A. **71**, 3–8 (2015). https://doi.org/10.1107/S2053273314026370
34. L.J. Farrugia, WinGX and ORTEP for windows: an update. J. Appl. Crystallogr. **45**, 849–854 (2012). https://doi.org/10.1107/S0021889812029111
35. R.O.V. Dolomanov, L.J. Bourhis, R.J. Gildea, J.A.K. Howard, H. Puschmann, OLEX2: a complete structure solution, refinement and analysis program. J. Appl. Crystallogr. **42**, 339–341 (2009). https://doi.org/10.1107/S0021889808042726
36. K. Brandenburg, H. Putz, Diamond version 3. Crystal Impact GbR, Postfach. **1251**, 53002 (2005)
37. J.W.M. Osterrieth, D.G.M. James Rampersad, N. Rampal, L. Skoric, B. Connolly, M. Allendorf, V. Stavila, J. Snider, R. Ameloot, J. Marreiros, C.O. Ania, D.C.S. Azevedo, E. Vilarrasa-García, B.F. Santos, X.-H. Bu, X. Zang, H. Bunzen, N.R. Champness, S.L. Griffin, B. Chen, R.-B. Lin, B. Coasne, S.M. Cohen, J.C. Moreton, Y.J. Colon, L. Chen, R. Clowes, F.-X. Coudert, Y. Cui, B. Hou, D. D'alessandro, P.W. Doheny, M. Dinca, C. Sun, C. Doonan, M. Huxley, J.D. Evans, P. Falcaro, R. Ricco, O.K. Farha, K.B. Idrees, T. Islamoglu, P. Feng, H. Yang, R. Forgan, D. Bara, S. Furukawa, E. Sanchez, J. Gascon, S. Telalovic, S.K. Ghosha, S. Mukherjee, M.R. Hill, M.M. Sadiq, P. Horcajada, P. Salcedo-Abraira, K. Kaneko, R. Kukobat, J. Kenvin, S. Keskin, S. Kitagawa, K. Otake, R.P. Lively, S.J.A. Dewitt, P.L. Llewellyn, B. Lotsch, S.T. Emmerling, A. Pütz, C. Martí-Gastaldo, N. Muñoz, J. Garcia-Martinez, N. Linares, D. Maspoch, J.A. Suarez, P. Moghadam, R. Oktavian, R. Morris, P. Wheatley, J. Navarro, C. Petit, D. Danaci, M. Rosseinsky, A. Katsoulidis, M. Schroder, X. Han, S. Yang, C. Serre, G. Mouchaham, D. Sholl, R. Thyagarajan, D. Siderius, R.Q. Snurr, R.B. Goncalves, V. Ting, J. Rowlandson, T. Uemura, T. Iiyuka, M. Van Der Veen, D. Rega, V. Vanspeybroeck, A. Lamaire, S. Rogge, K. Walton, L.W. Bingel, S. Wuttke, J. Andreo, O. Yaghi, B. Zhang, C. Yavuz, T. Nguyen, F. Zamora, C. Montoro, H.-C. Zhou, K. Angelo, D. Fairen-Jimenez, How reproducible are surface areas calculated from the BET equation? Adv. Mater. (2022). https://doi.org/10.1002/adma.202201502
38. Y.W. Abraha, C. Tsai, E.H.G. Langner, De novo syntheses of multi-linker Zn- and Co-based ZIFs with application in CO_2 fixation. Microporous Mesoporous Mater. **346**, 112319 (2022). https://doi.org/10.1016/j.micromeso.2022.112319
39. O. Karagiaridi, W. Bury, A.A. Sarjeant, C.L. Stern, O.K. Farha, J.T. Hupp, Synthesis and characterization of isostructural cadmium zeolitic imidazolate frameworks via solvent-assisted linker exchange. Chem. Sci. **3**, 3256–3260 (2012). https://doi.org/10.1039/c2sc20558k
40. K.C. Jayachandrababu, D.S. Sholl, S. Nair, Structural and mechanistic differences in mixed-linker zeolitic imidazolate framework synthesis by solvent assisted linker exchange and de novo routes. J. Am. Chem. Soc. **139**, 5906–5915 (2017). https://doi.org/10.1021/jacs.7b01660
41. P. Deria, J.E. Mondloch, O. Karagiaridi, W. Bury, J.T. Hupp, O.K. Farha, Beyond post-synthesis modification: evolution of metal-organic frameworks via building block replacement. Chem. Soc. Rev. **43**, 5896–5912 (2014). https://doi.org/10.1039/c4cs00067f
42. Y. Ban, Y. Li, X. Liu, Y. Peng, W. Yang, Solvothermal synthesis of mixed-ligand metal-organic framework ZIF-78 with controllable size and morphology. Microporous Mesoporous Mater. **173**, 29–36 (2013). https://doi.org/10.1016/j.micromeso.2013.01.031
43. C.R. Groom, I.J. Bruno, M.P. Lightfoot, S.C. Ward, The Cambridge structural database. Acta Crystallogr. Sect. B **72**, 171–179 (2016). https://doi.org/10.1107/S2052520616003954
44. G. Chaplais, G. Fraux, J.L. Paillaud, C. Marichal, H. Nouali, A.H. Fuchs, F.X. Coudert, J. Patarin, Impacts of the imidazolate linker substitution (CH_3, Cl, or Br) on the structural and adsorptive properties of ZIF-8. J. Phys. Chem. C. **122**, 26945–26955 (2018). https://doi.org/10.1021/acs.jpcc.8b08706
45. N. Novendra, J.M. Marrett, A.D. Katsenis, H.M. Titi, M. Arhangelskis, T. Friščić, A. Navrotsky, Linker substituents control the thermodynamic stability in metal-organic frameworks. J. Am. Chem. Soc. **142**, 21720–21729 (2020). https://doi.org/10.1021/jacs.0c09284
46. V.V. Butova, V.A. Polyakov, E.A. Bulanova, M.A. Soldatov, I.S. Yahia, H.Y. Zahran, A.F. Abd El-Rehim, H. Algarni, A.M. Aboraia, A.V. Soldatov, MW synthesis of ZIF-65 with a hierarchical porous structure. Microporous Mesoporous Mater. **293**, 109685 (2020). https://doi.org/10.1016/j.micromeso.2019.109685
47. Y. Choi, K. Noh, J. Lee, J. Kim, Porosity properties of the conformers of sodalite-like zeolitic imidazolate frameworks. J. Am. Chem. Soc. **140**, 14586–14589 (2018). https://doi.org/10.1021/jacs.8b08997
48. J.A. Boissonnault, A.G. Wong-Foy, A.J. Matzger, Core-shell structures arise naturally during ligand exchange in metal-organic frameworks. J. Am. Chem. Soc. **139**, 14841–14844 (2017). https://doi.org/10.1021/jacs.7b08349
49. H. Wu, R.S. Reali, D.A. Smith, M.C. Trachtenberg, J. Li, Highly selective CO_2 capture by a flexible microporous metal-organic framework (MMOF) material. Chem. Eur. J. **16**, 13951–13954 (2010). https://doi.org/10.1002/chem.201002683
50. N. Nijem, H. Wu, P. Canepa, A. Marti, K.J. Balkus, T. Thonhauser, J. Li, Y.J. Chabal, Tuning the gate opening pressure

of metal-organic frameworks (MOFs) for the selective separation of hydrocarbons. J. Am. Chem. Soc. **134**, 15201–15204 (2012). https://doi.org/10.1021/ja305754f
51. A. Boutin, F.-X. Coudert, M.-A. Springuel-Huet, A.V. Neimark, G. Ferey, A.H. Fuchs, The behavior of flexible MIL-53 (Al) upon CH_4 and CO_2 adsorption. J. Phys. Chem. C **114**, 22237–22244 (2010). https://doi.org/10.1021/jp108710h
52. S.A. Moggach, T.D. Bennett, A.K. Cheetham, The effect of pressure on ZIF-8: increasing pore size with pressure and the formation of a high-pressure phase at 1.47 GPa. Angew. Chemie Int. Ed. **48**, 7087–7089 (2009). https://doi.org/10.1002/anie.200902643
53. C.W. Tsai, E.H.G. Langner, R.A. Harris, Computational study of ZIF-8 analogues with electron donating and withdrawing groups for CO2 adsorption. Microporous Mesoporous Mater. **288**, 109613 (2019). https://doi.org/10.1016/j.micromeso.2019.109613
54. H.N. Abdelhamid, Removal of carbon dioxide using zeolitic imidazolate frameworks: adsorption and conversion via catalysis. Appl. Organomet. Chem. (2022). https://doi.org/10.1002/aoc.6753
55. A. Zanon, S. Chaemchuen, B. Mousavi, F. Verpoort, 1 Zn-doped ZIF-67 as catalyst for the CO_2 fixation into cyclic carbonates. J. CO2 Util. **20**, 282–291 (2017). https://doi.org/10.1016/j.jcou.2017.05.026
56. B. Olaniyan, B. Saha, Comparison of catalytic activity of ZIF-8 and Zr/ZIF-8 for greener synthesis of chloromethyl ethylene carbonate by CO_2 utilization. Energies **13**, 521 (2020). https://doi.org/10.3390/en13030521
57. J.A. Plumley, J.D. Evanseck, Periodic trends and index of boron lewis acidity. J. Phys. Chem. A **113**, 5985–5992 (2009). https://doi.org/10.1021/jp811202c
58. A.R. Jupp, T.C. Johnstone, D.W. Stephan, Improving the global electrophilicity index (GEI) as a measure of Lewis acidity. Inorg. Chem. **57**, 14764–14771 (2018). https://doi.org/10.1021/acs.inorgchem.8b02517
59. K.M. Bhin, J. Tharun, K.R. Roshan, D.W. Kim, Y. Chung, D.W. Park, Catalytic performance of zeolitic imidazolate framework ZIF-95 for the solventless synthesis of cyclic carbonates from CO_2 and epoxides. J. CO2 Util. **17**, 112–118 (2017). https://doi.org/10.1016/j.jcou.2016.12.001
60. H. Ryu, R. Roshan, M. Il Kim, D.W. Kim, M. Selvaraj, D.W. Park, Cycloaddition of carbon dioxide with propylene oxide using zeolitic imidazolate framework ZIF-23 as a catalyst. Korean J. Chem. Eng. **34**, 928–934 (2017). https://doi.org/10.1007/s11814-016-0339-4
61. R.R. Kuruppathparambil, R. Babu, H.M. Jeong, G.Y. Hwang, G.S. Jeong, M. Il Kim, D.W. Kim, D.W. Park, A solid solution zeolitic imidazolate framework as a room temperature efficient catalyst for the chemical fixation of CO_2. Green Chem. **18**, 6349–6356 (2016). https://doi.org/10.1039/c6gc01614f
62. R.R. Kuruppathparambil, T. Jose, R. Babu, G.Y. Hwang, A.C. Kathalikkattil, D.W. Kim, D.W. Park, A room temperature synthesizable and environmental friendly heterogeneous ZIF-67 catalyst for the solvent less and co-catalyst free synthesis of cyclic carbonates. Appl. Catal. B **182**, 562–569 (2016). https://doi.org/10.1016/j.apcatb.2015.10.005
63. T. Jose, Y. Hwang, D.W. Kim, M. Il Kim, D.W. Park, Functionalized zeolitic imidazolate framework F-ZIF-90 as efficient catalyst for the cycloaddition of carbon dioxide to allyl glycidyl ether. Catal. Today. **245**, 61–67 (2015). https://doi.org/10.1016/j.cattod.2014.05.022
64. R. Babu, S.H. Kim, J.F. Kurisingal, H.J. Kim, G.G. Choi, D.W. Park, A room temperature synthesizable zeolitic imidazolium framework catalyst for the solvent-free synthesis of cyclic carbonates. J. CO2 Util. **25**, 6–13 (2018). https://doi.org/10.1016/j.jcou.2018.03.006